OPEN

Renal Cyst Pseudoenhancement: Intraindividual Comparison Between Virtual Monochromatic Spectral Images and Conventional Polychromatic 120-kVp Images Obtained During the Same CT Examination and Comparisons Among Images Reconstructed Using Filtered Back Projection, Adaptive Statistical Iterative Reconstruction, and Model-Based Iterative Reconstruction

Yoshitake Yamada, MD, PhD, Minoru Yamada, PhD, Koichi Sugisawa, RT, Hirotaka Akita, MD, Eisuke Shiomi, MD, Takayuki Abe, PhD, Shigeo Okuda, MD, PhD, and Masahiro Jinzaki, MD, PhD

Abstract: The purpose of this study was to compare renal cyst pseudoenhancement between virtual monochromatic spectral (VMS) and conventional polychromatic 120-kVp images obtained during the same abdominal computed tomography (CT) examination and among images reconstructed using filtered back projection (FBP), adaptive statistical iterative reconstruction (ASIR), and model-based iterative reconstruction (MBIR).

Our institutional review board approved this prospective study; each participant provided written informed consent. Thirty-one patients (19 men, 12 women; age range, 59–85 years; mean age, 73.2 ± 5.5 years) with renal cysts underwent unenhanced 120-kVp CT followed by sequential fast kVp-switching dual-energy (80/140 kVp) and 120-kVp abdominal enhanced CT in the nephrographic phase over a 10-cm scan length with a random acquisition order and 4.5-second intervals. Fifty-one renal cysts (maximal diameter, 18.0 ± 14.7 mm [range, 4–61 mm]) were identified. The CT attenuation values of the cysts as well as of the kidneys were measured on the unenhanced images, enhanced VMS images (at 70 keV) reconstructed using FBP and ASIR from dual-energy data, and enhanced 120-kVp images reconstructed using FBP, ASIR, and MBIR. The results were analyzed using the mixed-effects model and paired *t* test with Bonferroni correction.

The attenuation increases (pseudoenhancement) of the renal cysts on the VMS images reconstructed using FBP/ASIR (least square mean, 5.0/6.0 Hounsfield units [HU]; 95% confidence interval, 2.6–7.4/3.6–8.4 HU) were significantly lower than those on the conventional 120-kVp images reconstructed using FBP/ASIR/MBIR (least square mean, 12.1/12.8/11.8 HU; 95% confidence interval, 9.8–14.5/10.4–15.1/9.4–14.2 HU) (all $P < .001$); on the other hand, the CT attenuation values of the kidneys on the VMS images were comparable to those on the 120-kVp images.

Regardless of the reconstruction algorithm, 70-keV VMS images showed a lower degree of pseudoenhancement of renal cysts than 120-kVp images, while maintaining kidney contrast enhancement comparable to that on 120-kVp images.

(*Medicine* 94(15):e754)

Abbreviations: ASIR = adaptive statistical iterative reconstruction, FBP = filtered back projection, IR = iterative reconstruction, MBIR = model-based iterative reconstruction, VMS = virtual monochromatic spectral.

Editor: Takayuki Masui.
Received: January 19, 2015; revised: March 15, 2015; accepted: March 17, 2015.
From the Department of Diagnostic Radiology (YY, KS, HA, ES, SO, MJ), Keio University School of Medicine; Multi-dimension Biomedical Imaging & Information Laboratory in Research Park (MY), Keio University School of Medicine; and Department of Preventive Medicine and Public Health, Center for Clinical Research, Keio University School of Medicine (TA), Shinjuku-ku, Tokyo, Japan.
Correspondence: Masahiro Jinzaki, Department of Diagnostic Radiology, Keio University School of Medicine, 35, Shinanomachi, Shinjuku-ku, Tokyo, 160-8582, Japan (e-mail: jinzaki@rad.med.keio.ac.jp).
This study was supported in part by JSPS KAKENHI Grant Number 23591795 and 26861016. Masahiro Jinzaki received a grant from GE Healthcare Japan. The remaining authors (YY, MY, KS, HA, ES, TA, and SO) have no financial disclosures to make and had complete unrestricted access to the study data at all stages of the study. None of the authors are employees of GE Healthcare or received individual industry funding for this project.

ISSN: 0025-7974
DOI: 10.1097/MD.0000000000000754

INTRODUCTION

A critical diagnostic criterion for differentiating a solid renal mass from a benign cyst is the presence of enhancement after intravenous contrast administration.[1–5] In computed tomography (CT), an increase of the density by at least 10 Hounsfield units (HU) in a renal lesion has been proposed to suggest enhancement and to indicate a solid renal mass.[1–5] However, although simple cysts are not enhancing, attenuation increase may erroneously suggest enhancement, particularly in the case of small renal cysts, because of pseudoenhancement and partial volume averaging.[4–9] Renal cyst pseudoenhancement refers to artifactual increase in the attenuation of a simple renal cyst following contrast material administration, even after removal of the effects of partial volume averaging.[4–9] Pseudoenhancement is thought to be a consequence of the beam-hardening effect of the enhancing renal parenchyma combined with inadequate correction.[3,6,9,10]

The recently developed fast kVp-switching dual-energy CT technology enables almost simultaneous dual-energy CT data acquisition with a single tube and a single detector,[11] and provides virtual monochromatic spectral (VMS) images. As compared to the widely used polychromatic imaging (ie, 120 kVp), VMS images reconstructed with more accurate beam-hardening correction using 2 basis materials (water and iodine) provide improved linearity of the CT attenuation.[11–18] Although VMS images showed a lower degree of pseudoenhancement of renal cysts than 120-kVp images in a phantom study,[19] to the best of our knowledge, no clinical study to date has compared renal cyst pseudoenhancement between VMS and conventional polychromatic 120-kVp imaging obtained simultaneously in the same patients. Furthermore, no clinical study has assessed the effect of the iterative reconstruction (IR) technique on renal cyst pseudoenhancement.

The purpose of this study was to compare renal cyst pseudoenhancement between VMS and conventional polychromatic 120-kVp images obtained during the same abdominal CT examination and among images reconstructed using filtered back projection (FBP), adaptive statistical iterative reconstruction (ASIR), and model-based iterative reconstruction (MBIR).

METHODS

Patients and Renal Cysts

This prospective study was conducted with the approval of our institutional review board, and written informed consent was obtained from each of the patients. From August 2011 to September 2011, 36 consecutive patients who met the following inclusion criteria for the study were recruited: age equal to or greater than 55 years, known to have renal cysts, and scheduled for unenhanced and contrast-enhanced abdominal CT as part of clinical standard of care on a specific scanner. Patients were excluded if they were younger than 55 years, were pregnant, potentially pregnant or lactating, had any contraindication to administration of iodinated contrast material, such as a previous history of anaphylactoid reaction, had renal failure (serum creatinine level >2.0 mg/dL [177 μmol/L]) or did not provide written informed consent; 5 of the 36 patients did not wish to participate in the study and refused to provide informed consent. Therefore, images from the remaining 31 patients (19 men, 12 women; age range, 59–85 years; mean age, 73.2 ± 5.5 years) were finally included in the analysis. The clinical indications for routine standard-of-care CT in the subjects of this study were staging or restaging of known malignancy (n = 29) and suspected malignancy (n = 2). Fifty-one renal cysts (maximal diameter, 18.0 ± 14.7 mm [range 4–61 mm]) were identified in the research images described below, by interpretation of both the standard-of-care and research images. Proof of renal cysts was based on the lesions showing no change in size as compared to that in the previous or subsequent CT examinations; the follow-up periods were 807.5 ± 237.2 days (range, 385–1279 days). The 51 renal cysts were further classified according to the percentage of the cyst perimeter surrounded by the renal parenchyma (<25%, 13 renal cysts; 25% to 50%, 11 renal cysts; 51% to 75%, 9 renal cysts; >75%, 18 renal cysts), as described previously,[2,5] as a variable representing the relationship to the renal parenchyma. The heights and weights of the patients were measured, and the body mass index (BMI) was calculated (weight in kilograms divided by height squared in meters).

Imaging Protocol

First, a clinically indicated standard-of-care unenhanced abdominal 120-kVp CT including the level of the liver and kidneys was performed using the Discovery CT750 HD scanner (GE Healthcare, Waukesha, WI) under the following scanning parameters: tube current, 480 mA; detector collimation 0.625 × 64 mm; rotation speed, 0.5 seconds; pitch factor, 1.375; volume CT dose index, 13 mGy; scan field of view (FOV), 500 mm. Then, a clinically indicated standard-of-care portal-dominant phase contrast-enhanced abdominal CT examination was performed, 70 seconds after the injection of iohexol (Omnipaque 300; Daiichi-Sankyo, Japan) at the dose of 2.0 mL/kg using a power injector at the rate of 2 mL/s via the median cubital vein. Subsequently, 90 seconds after the administration of the contrast medium (nephrographic phase), sequential fast kVp-switching dual-energy (80/140 kVp) and single-energy (120 kVp) enhanced abdominal CT (or sequential single-energy and dual-energy CT) were performed for research purposes during a single breath-hold over a 10-cm scan length at the level of the kidneys, using a random acquisition order to avoid contrast enhancement bias caused by delay in scanning after the start of the injection. The interval between the start of the 2 research scans was 4.5 seconds, which was the minimum setting. The other scanning parameters for fast kVp-switching between 80 and 140 kVp were as follows: tube current, 630 mA; detector collimation 0.625 × 64 mm; rotation speed, 0.5 seconds; pitch factor, 1.375; volume CT dose index, 13 mGy; scan FOV, 500 mm. The other scanning parameters for 120-kVp single-energy CT were as follows: tube current, 480 mA; detector collimation 0.625 × 64 mm; rotation speed, 0.5 seconds; pitch factor, 1.375; volume CT dose index, 13 mGy (the same as those for dual-energy CT); scan FOV, 500 mm. We therefore had 3 raw data files (unenhanced 120-kVp CT, fast kVp-switching dual-energy contrast-enhanced CT in the nephrographic phase, and 120-kVp single-energy contrast-enhanced CT in the nephrographic phase) at the level of the kidneys for all the patients. The effective dose estimate for the 2 research scans was 6.8 mSv, which was determined based on the dose length product measurements and previously reported appropriate normalized coefficients for abdominal CT (0.015 mSv/[mGy cm]).[20]

Image Reconstruction

Six image series were created for each patient (Figure 1). A series of contiguous 2.5-mm-thick unenhanced 120-kVp CT images reconstructed using FBP (Figure 1A) were generated from the unenhanced 120-kVp CT data. Next, a series of contiguous 2.5-mm-thick contrast-enhanced 120-kVp images reconstructed using FBP (120-kVp-FBP), ASIR (so-called hybrid IR) (120-kVp-ASIR), and MBIR (so-called pure IR) (120-kVp-MBIR) were generated from the enhanced single-energy CT data with the standard kernel (Figure 1B, C, and D, respectively). The series of contiguous 2.5-mm-thick contrast-enhanced VMS images reconstructed using FBP (VMS-FBP) and ASIR (VMS-ASIR) at 70 keV were generated from the enhanced dual-energy CT data with the standard kernel (Figure 1E and F, respectively). The choice of 70 keV was based on previous phantom and clinical studies, which showed that VMS images at approximately 70 keV yielded the lowest image noise and the highest contrast-to-noise ratio (CNR) among the 101 sets of VMS images in the range of 40 to 140 keV at 1-keV intervals[14,17] and also showed that the CT attenuation values of the VMS images at approximately 70 keV were equal to those of the 120-kVp CT images.[14,18,21] We used 50% ASIR, which means that 50% of the ASIR image was blended with the FBP image, for both the 120-kVp-ASIR and

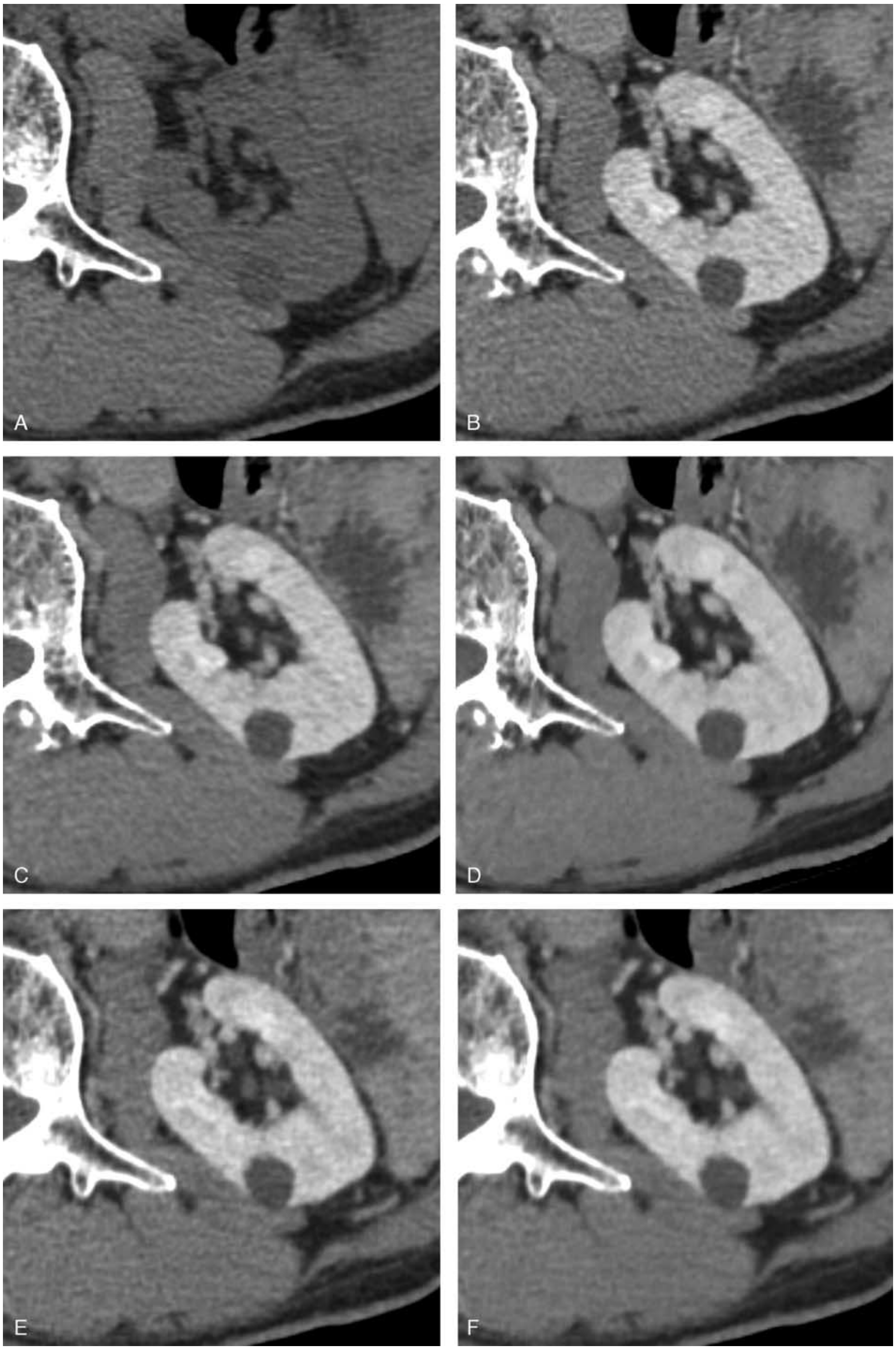

FIGURE 1. Transverse abdominal CT images obtained in a 71-year-old man weighing 61 kg with a left renal cyst: (A) unenhanced 120-kVp CT images reconstructed using filtered back projection (FBP); (B) contrast-enhanced 120-kVp images reconstructed using FBP (120-kVp-FBP images); (C) contrast-enhanced 120-kVp images reconstructed using adaptive statistical iterative reconstruction (120-kVp-ASIR images); (D) contrast-enhanced 120-kVp images reconstructed using model-based iterative reconstruction (120-kVp-MBIR image); (E) contrast-enhanced virtual monochromatic spectral (VMS) images reconstructed using FBP (VMS-FBP image); (F) contrast-enhanced VMS images reconstructed using ASIR (VMS-ASIR images).

VMS-ASIR images. The choice of the 50% ASIR was based on the results of previous studies.[22,23] Finally, we obtained 186 sets of 2.5-mm-thick images, that is, 31 image sets each of unenhanced 120-kVp with FBP, contrast-enhanced 120-kVp-FBP, 120-kVp-ASIR, 120-kVp-MBIR, VMS-FBP, and VMS-ASIR images (Figure 1). At the present time, the MBIR technique cannot be applied to VMS images. The display FOVs were approximately 350 mm for all the images.

Attenuation Increase (Postcontrast HU Increase)

Two board-certified radiologists with 8 and 23 years of experience in interpreting abdominal CT images placed, by consensus, a circular or ovoid region of interest (ROI) in each renal cyst on unenhanced 120-kVp, contrast-enhanced 120-kVp-FBP, 120-kVp-ASIR, 120-kVP-MBIR, VMS-FBP, and VMS-ASIR images, using an independent workstation (Advantage workstation 4.5; GE Healthcare). The ROIs were drawn to cover approximately one-half of the diameter of each cyst to minimize the partial volume artifact[3,4] (we also attempted to exclude the effect of the partial volume artifact on attenuation increase by using thin 2.5-mm-thick images).[9] The size, shape, and position of the ROIs were kept constant, to the extent possible, among the 6 protocols by applying the copy-and-paste function at the workstation; however, in case of misregistration between unenhanced and enhanced protocols due to differences in the depth of the breath-holds or movement of the patient during the intravenous needle insertion procedure, the positions of the ROIs were visually adjusted. Attenuation increase was expressed as the difference in the CT attenuation values of each cyst between the unenhanced 120-kVp images and contrast-enhanced 120-kVp-FBP, 120-kVp-ASIR, 120-kVP-MBIR, VMS-FBP, and VMS-ASIR images. The percentage of renal cysts showing an attenuation increase of more than 10 HU was also calculated for each image protocol, as described previously.[3,4,7,10] The default abdominal window setting (window width, 400 HU; window level, 40 HU) were used for the ROI measurements.

CT Attenuation Values, Image Noises in the Bilateral Kidneys, and Cyst-to-Kidney CNR

Two board-certified radiologists with 8 and 23 years of experience in interpreting abdominal CT also placed, by consensus, a circular or ovoid ROI in the bilateral kidneys (renal cortex). The CT attenuation values (HU) and objective image noise (ie., standard deviation [SD]) were measured in the contrast-enhanced 120-kVp-FBP, 120-kVp-ASIR, 120-kVP-MBIR, VMS-FBP, and VMS-ASIR images using the independent workstation (Advantage workstation 4.5). A constant size of the ROI of approximately 1.0 cm^2 was used as much as possible at all the sites. The size, shape, and position of the ROIs were kept constant among the 5 protocols by applying a copy-and-paste function at the workstation. The cyst-to-kidney CNRs were calculated using the following formula[17,18,24,25]:

$$\mathrm{CNR}_{\text{cyst-to-kidney}} = |\mathrm{ROI}_{\text{cyst}} - \mathrm{ROI}_{\text{kidney}}|/\mathrm{SD}_{\text{kidney}},$$

where $\mathrm{ROI}_{\text{kidney}}$ and $\mathrm{ROI}_{\text{cyst}}$ denote the CT attenuation values of the kidneys and renal cysts, and $\mathrm{SD}_{\text{kidney}}$ denotes the image noise of the kidneys.

Statistical Analysis

A general linear mixed-effects model containing the image reconstruction protocol as a fixed effect and the patient as a random effect was used to compare the attenuation increases and the cyst-to-kidney CNRs among the images obtained using the different reconstruction protocols. The degree of freedom was approximated by the Satterthwaite method. A paired *t* test was used to compare the CT attenuation values and objective image noises among the images obtained using the different reconstruction protocols. The Bonferroni correction was used for all multiple comparisons. The effects of the cyst diameter and relationship to the renal parenchyma on the attenuation increase were also evaluated using a mixed-effects model (image reconstruction protocol, diameter, and relationship to the renal parenchyma as fixed effects; patient as a random effect). The significance level for all tests was 5% (2 sided). Data were analyzed using commercially available software programs (SPSS version 21, IBM SPSS, Armonk, New York; SAS version 9.1, SAS, Cary, NC).

RESULTS

Patient Characteristics

The mean height, weight, and BMI of the 31 patients were 161.5 ± 9.3 cm (range, 140.0–180.0 cm), 57.8 ± 8.7 kg (range, 40.0–83.0 kg), and 22.1 ± 2.7 kg/m^2 (range, 18.3–27.5 kg/m^2), respectively.

Attenuation Increases and CT Attenuation Values of the Kidney

The attenuation increases on the VMS-FBP and VMS-ASIR images (least square mean ± standard error, 5.0 ± 1.2 and 6.0 ± 1.2 HU, respectively; 95% confidence interval, 2.6–7.4 and 3.6–8.4 HU, respectively) were significantly lower than those on the conventional 120-kVp-FBP, 120-kVp-ASIR, and 120-kVp-MBIR images (least square mean ± standard error, 12.1 ± 1.2, 12.8 ± 1.2, and 11.8 ± 1.2 HU, respectively; 95% confidence interval, 9.8–14.5, 10.4–15.1, and 9.4–14.2 HU, respectively) (all $P < .001$) (Figure 2), while the CT attenuation values of the kidneys of both sides on the VMS-FBP (mean ± standard deviation, 180.5 ± 18.1 HU [right]; 181.6 ± 20.9 HU [left]) and VMS-ASIR images (179.8 ± 18.2 HU [right]; 180.8 ± 20.7 HU [left]) were comparable to those on the 120-kVp-FBP (178.9 ± 19.8 HU [right]; 180.5 ± 21.9 HU [left]), 120-kVp-ASIR (178.9 ± 19.7 HU [right]; 180.3 ± 21.8 HU [left]), and 120-kVp-MBIR images (179.9 ± 19.3 HU [right]; 181.5 ± 22.0 HU [left]) (Figure 3). There was no significant difference in the attenuation increase between the VMS-FBP and VMS-ASIR images, and also no significant differences in the attenuation increase among the 120-kVp-FBP, 120-kVp-ASIR, and 120-kVp-MBIR images (Figure 2). The percentages of renal cysts showing an attenuation increase of more than 10 HU were 43.1%, 45.1%, 45.1%, 5.9%, and 9.8% on the 120-kVp-FBP, 120-kVp-ASIR, 120-kVp-MBIR, VMS-FBP, and VMS-ASIR images, respectively. The CT attenuation values of the kidneys of both sides were significantly lower on the VMS-ASIR images than on the VMS-FBP images; however, the differences were less than 1 HU (Figure 3). There were no significant differences in the CT attenuation values of the kidneys of either side among the 120-kVp-FBP, 120-kVp-ASIR, and 120-kVp-MBIR images (Figure 3).

Effects of the Cyst Diameter and Relationship to the Renal Parenchyma on the Attenuation Increase

In addition to the effect of the image reconstruction protocol, a smaller cyst diameter was associated with a significantly higher attenuation increase ($P = .0093$), while relationship to the renal parenchyma (the proportion of the cyst perimeter surrounded by the renal parenchyma) did not have any significant effect on the attenuation increase ($P = .6610$) (Table 1).

Image Noises in the Bilateral Kidneys and the Cyst-to-Kidney CNRs

The objective image noises in the bilateral kidneys on the VMS-ASIR and 120-kVp-MBIR images were significantly lower than those on the 120-kVp-FBP and 120-kVp-ASIR

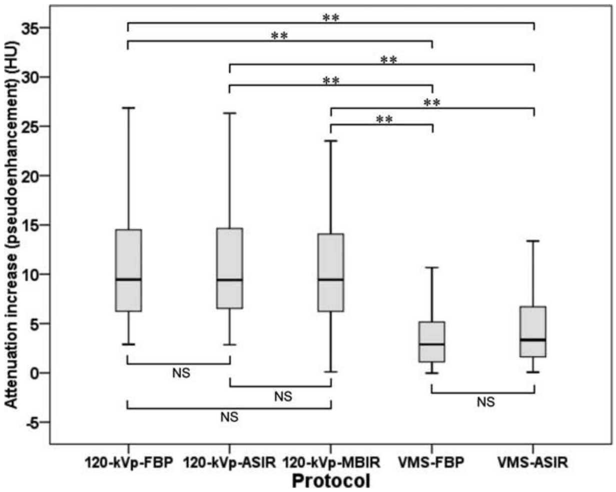

FIGURE 2. Attenuation increase (HU) on 120-kVp-FBP, 120-kVp-ASIR, 120-kVp-MBIR, VMS-FBP, and VMS-ASIR images expressed as medians. Boxes: upper to lower quartile. Thin lines: maximum and minimum (excluding outliers and extreme values). A general linear mixed-effects model was used to compare the attenuation increase among the images obtained using the different reconstruction protocols. $P < .005$ was considered to indicate statistically significant difference with Bonferroni correction for multiple comparisons. $^{*} = P < .005$. $^{**} = P < .0001$, 120-kVp-ASIR = contrast-enhanced 120-kVp images reconstructed using adaptive statistical iterative reconstruction, 120-kVp-FBP = contrast-enhanced 120-kVp images reconstructed using filtered back projection, 120-kVp-MBIR = contrast-enhanced 120-kVp images reconstructed using model-based iterative reconstruction, VMS-ASIR = contrast-enhanced virtual monochromatic spectral images (at 70 keV) reconstructed using adaptive statistical iterative reconstruction, VMS-FBP = contrast-enhanced virtual monochromatic spectral images (at 70 keV) reconstructed using filtered back projection, NS = not significant.

images (all $P < 0.005$), and there was no significant difference in the objective image noise in the bilateral kidneys between the VMS-ASIR and 120-kVp-MBIR images (Figure 4).

The cyst-to-kidney CNR was the highest on the 120-kVp-MBIR images (all $P < 0.005$); also, the cyst-to-kidney CNR on the VMS-ASIR images was higher than the values on 120-kVp-FBP, 120-kVp-ASIR, and VMS-FBP images (Figure 5).

DISCUSSION

In this prospective clinical study, we demonstrated that VMS images showed a lower degree of pseudoenhancement of renal cysts than 120-kVp images in the same patients, regardless of the reconstruction algorithm. These findings are important because they indicate the possibility of easier differentiation of renal cysts from renal tumors using VMS imaging in the clinical setting.

Renal cyst pseudoenhancement is strongly associated with the beam-hardening effect and the pseudoenhancement is believed to be a consequence of inadequate correction of beam-hardening artifacts.[3,6,9,10,19] In the fast kVp-switching dual-energy CT used in this study, coherent high-kVp and low-kVp projections are mapped into material density projections of the selected basis material pair (water and iodine).[11–13,16,18] With the use of these 2 basis materials, beam-hardening correction for the basis material enables

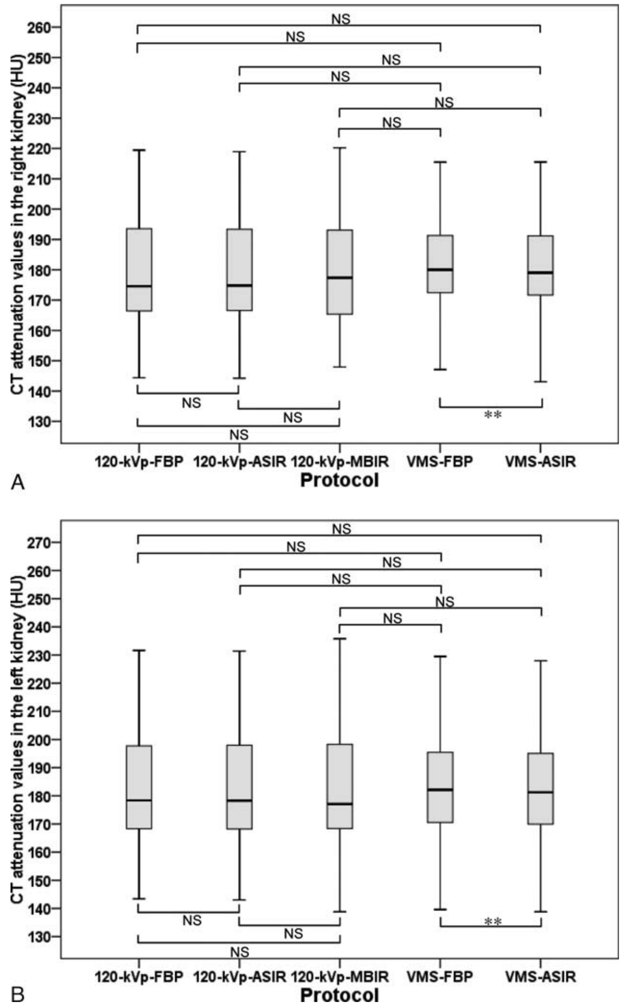

FIGURE 3. CT attenuation values (HU) on contrast-enhanced 120-kVp-FBP, 120-kVp-ASIR, 120-kVp-MBIR, VMS-FBP, and VMS-ASIR images expressed as medians: (A) right kidney; (B) left kidney. Boxes: upper to lower quartile. Thin lines: maximum and minimum (excluding outliers and extreme values). A paired *t* test was used to compare the CT attenuation values among the images obtained using the different reconstruction protocols. $P < .005$ was considered to indicate statistically significant difference with Bonferroni correction for multiple comparisons. $^{*} = P < .005$. $^{**} = P < .0001$, 120-kVp-ASIR = contrast-enhanced 120-kVp images reconstructed using adaptive statistical iterative reconstruction, 120-kVp-FBP = contrast-enhanced 120-kVp images reconstructed using filtered back projection, 120-kVp-MBIR = contrast-enhanced 120-kVp images reconstructed using model-based iterative reconstruction, VMS-ASIR = contrast-enhanced virtual monochromatic spectral images (at 70 keV) reconstructed using adaptive statistical iterative reconstruction, VMS-FBP = contrast-enhanced virtual monochromatic spectral images (at 70 keV) reconstructed using filtered back projection, NS = not significant.

accurate basis material decomposition. This means that the beam-hardening correction for the iodine data is performed using iodine and that for the water data is performed using water, while in single-energy CT, the beam-hardening effect is corrected using only 1 material.[11–13,18] Thus, more accurate beam-hardening correction using 2 materials (water and iodine) allows for improved linearity of CT attenuation, which would

TABLE 1. Analysis of Variance (ANOVA) Using a Mixed-Effects Model to Determine the Effects on Attenuation Increase of the Cyst Diameter and Relationship to the Renal Parenchyma

Variable	Estimate	Standard Error	Degree Of Freedom	*t* Value	*P* Value
Intercept	7.6311	1.7603	131	4.34	<.0001
(120-kVp-FBP−VMS-ASIR)	(6.1582)	(0.7320)	(217)	(8.41)	(<.0001)
(120-kVp-ASIR−VMS-ASIR)	(6.7822)	(0.7320)	(217)	(9.26)	(<.0001)
(120-kVp-MBIR−VMS-ASIR)	(5.8365)	(0.7320)	(217)	(7.97)	(<.0001)
(VMS-FBP−VMS-ASIR)	(−1.0000)	(0.7320)	(217)	(−1.37)	(.1733)
Diameter	−0.0681	0.0260	233	−2.62	.0093
Relationship to the renal parenchyma	−0.1726	0.3932	247	−0.44	.6610

120-kVp-ASIR = contrast-enhanced 120-kVp images reconstructed using adaptive statistical iterative reconstruction, 120-kVp-FBP = contrast-enhanced 120-kVp images reconstructed using filtered back projection, 120-kVp-MBIR = contrast-enhanced 120-kVp images reconstructed using model-based iterative reconstruction, VMS-ASIR = contrast-enhanced virtual monochromatic spectral images (at 70 keV) reconstructed using adaptive statistical iterative reconstruction, VMS-FBP = contrast-enhanced virtual monochromatic spectral images (at 70 keV) reconstructed using filtered back projection.

result in a lower degree of pseudoenhancement of renal cysts on VMS images.

In a previous phantom study conducted by Jung et al, the attenuation increase (pseudoenhancement) of renal cysts on VMS images at 70 keV (21.51 ± 6.18 HU) was lower than that on 120-kVp images (42.44 ± 4.03 HU), examined using a saline-filled tapering cylindrical cyst model suspended in the kidney phantoms (7 × 7 × 20 cm) filled with 40- and 240-HU solutions of diluted contrast material, mimicking the unenhanced phase and nephrographic phase of MDCT, respectively.[19] As compared to the finding in the previous phantom study, our clinical study revealed that the pseudoenhancement of renal cysts on VMS-FBP images was lower (least square mean ± standard error, 5.0 ± 1.2 HU) and that on 120-kVp-FBP images was also lower (least square mean ± standard error, 12.1 ± 1.2 HU). Two possible explanations are that the cylindrical cyst model used in the previous phantom study[19] was entirely surrounded by diluted contrast material (not simulating the renal hilus, renal pelvis, or the renal sinus fat) and the CT attenuation values of the kidney phantoms filled with 240-HU solutions of diluted contrast material in the previous study were higher than those of the kidneys in our clinical study (mean, approximately 180 HU), which would be expected to exert a greater beam-hardening effect and result in the higher pseudoenhancement observed in their phantom study as compared to that noted in our clinical study. Nevertheless, the trend of our clinical results of the lower degree of pseudoenhancement on the VMS images as compared to that on the 120-kVp images is consistent with the results of the previous phantom study.[19] Another previous study conducted by Mileto et al reported that pseudoenhancement (attenuation increase of more than 10 HU) never occurred on VMS images at energy levels ranging from 90 to 140 keV and that the patient body size had a significant effect on the selection of the optimal monochromatic energy level.[26] On the other hand, our results showed that in the 70-keV VMS images, more than 90% of the renal cysts showed attenuation increase of less than 10 HU, while the CT attenuation values of the kidneys were comparable to those on the 120-kVp images. One possible reason for this result is that the patients in this study, with a mean BMI of 22.1 ± 2.7 kg/m^2 (range, 18.3–27.5 kg/m^2) were relatively smaller than those in the aforementioned study reported by Mileto et al, who had a mean BMI of 31.3 ± 6.2 kg/m^2 (range, 20.1–42.9 kg/m^2). Considering our results, especially in patients with BMI < 27 kg/ m^2, 70-keV VMS images would be the optimal choice not only for differentiating renal cysts from renal tumors, but also for interpreting the whole of abdominal CT, because 80- to 140-keV VMS images show lower contrast enhancement of the abdominal solid organs as compared to 120-kVp images.[17] Furthermore, Mileto et al compared VMS images with 140-kVp images in their clinical evaluations, while in the current study, we compared VMS images with 120-kVp images; 120 kVp images have been widely used as the standard acquisition condition in CT ever since the introduction of CT in clinical diagnostics.

Our results also showed that a smaller cyst diameter was associated with significantly higher attenuation increase (pseudoenhancement), which is consistent with the results of several phantom and clinical studies reported previously.[3–6,8,27] Furthermore, our results suggest that the image reconstruction protocol (120-kVp images or VMS images) has a stronger influence on pseudoenhancement than the cyst diameter. On the other hand, the relationship of the cyst to the renal parenchyma (location) did not have any significant effect on pseudoenhancement, which is also consistent with the results of previous clinical studies.[2,3] However, the effect of the location of the renal cyst on the degree of pseudoenhancement remains controversial, since some previous studies have reported the existence of a correlation between the location of renal cysts and the level of pseudoenhancement.[4,5]

In this study, the CT attenuation values of the kidneys of both sides were significantly lower on the VMS-ASIR images than on the VMS-FBP images, although the differences were less than 1 HU, and we have not been able to come up with a reasonable explanation for this slight difference. Nonetheless, the differences were far less than 1% (less than 1 HU/approximatly180 HU).

MBIR (pure IR), which takes into account an accurate system model,[28] statistical noise model,[29] and a prior model,[30] provides improved image quality with much lower image noise and higher CNR as compared to FBP and ASIR.[31,32] Our study revealed that the cyst-to-kidney CNR was the highest on 120-kVp-MBIR images, and that the objective image noises in the kidneys on 120−kVp-MBIR images were significantly lower than those on 120-kVp-FBP and 120-kVp-ASIR images, which are consistent with previous reports.[32,33] However, we also found no significant differences of the attenuation increase among 120-kVp-FBP, 120-kVp-ASIR, and 120-kVp-MBIR images; that is, MBIR and ASIR had little effect on the degree of pseudoenhancement of renal cysts. Our results suggest that

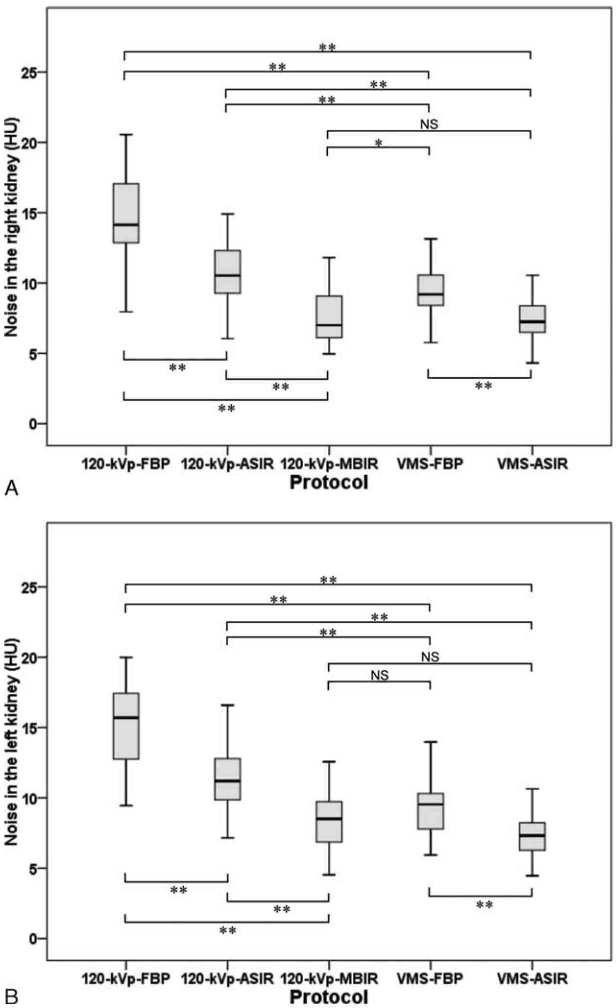

FIGURE 4. Objective image noise on contrast-enhanced 120-kVp-FBP, 120-kVp-ASIR, 120-kVp-MBIR, VMS-FBP, and VMS-ASIR images expressed as medians: (A) right kidney; (B) left kidney. Boxes: upper to lower quartile. Thin lines: maximum and minimum (excluding outliers and extreme values). A paired *t* test was used to compare the objective image noise among the images obtained using the different reconstruction protocols. $P < .005$ was considered to indicate statistically significant difference with Bonferroni correction for multiple comparisons. $^{*} = P < .005$. $^{**} = P < .0001$, 120-kVp-ASIR = contrast-enhanced 120-kVp images reconstructed using adaptive statistical iterative reconstruction, 120-kVp-FBP = contrast-enhanced 120-kVp images reconstructed using filtered back projection, 120-kVp-MBIR = contrast-enhanced 120-kVp images reconstructed using model-based iterative reconstruction, VMS-ASIR = contrast-enhanced virtual monochromatic spectral images (at 70 keV) reconstructed using adaptive statistical iterative reconstruction, VMS-FBP = contrast-enhanced virtual monochromatic spectral images (at 70 keV) reconstructed using filtered back projection, NS = not significant.

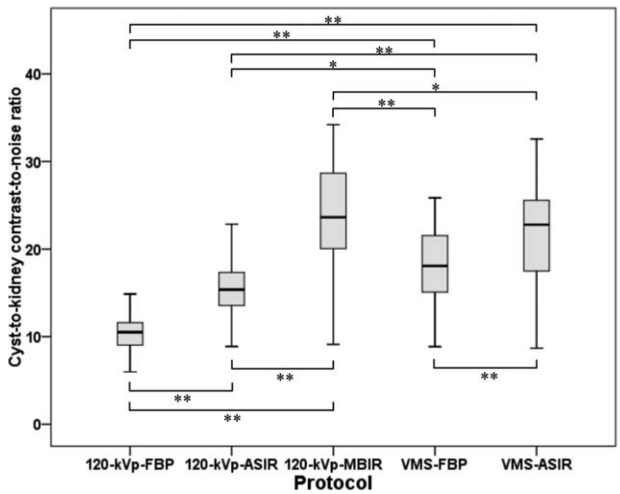

FIGURE 5. Cyst-to-kidney contrast-to-noise ratios on contrast-enhanced 120-kVp-FBP, 120-kVp-ASIR, 120-kVp-MBIR, VMS-FBP, and VMS-ASIR images expressed as medians. Boxes: upper to lower quartile. Thin lines: maximum and minimum (excluding outliers and extreme values). A general linear mixed-effects model was used to compare the cyst-to-kidney contrast-to-noise ratios among the images obtained using the different reconstruction protocols. $P < .005$ was considered to indicate statistically significant difference with Bonferroni correction for multiple comparisons. $^{*} = P < .005$. $^{**} = P < .0001$, 120-kVp-ASIR = contrast-enhanced 120-kVp images reconstructed using adaptive statistical iterative reconstruction, 120-kVp-FBP = contrast-enhanced 120-kVp images reconstructed using filtered back projection, 120-kVp-MBIR = contrast-enhanced 120-kVp images reconstructed using model-based iterative reconstruction, VMS-ASIR = contrast-enhanced virtual monochromatic spectral images (at 70 keV) reconstructed using adaptive statistical iterative reconstruction, VMS-FBP = contrast-enhanced virtual monochromatic spectral images (at 70 keV) reconstructed using filtered back projection, NS = not significant.

once the CT images are acquired with single-energy (polychromatic 120-kVp) x-rays, the IR technique cannot provide sufficient correction for the beam-hardening effect. Furthermore, MBIR for 120-kVp CT currently requires between 30 and 60 minutes for reconstruction of the 500 to 600 images obtained for a single patient, which would limit its application for routine CT examination.[32,34] On the other hand, VMS-FBP and VMS-ASIR require approximately 3 and 4 minutes, respectively, for reconstruction of the 500 to 600 images obtained for a single patient.[18] In addition to accurate differentiation between renal cysts and solid masses, in terms of the reconstruction time, VMS-FBP and VMS-ASIR images would be more useful than 120-kVp-MBIR images in routine clinical practice.

Our study had several limitations. First, we included only 31 patients, and further studies in larger patient populations are required to confirm these preliminary findings. Second, at the present time, the MBIR technique cannot be applied to VMS images. We found that the cyst-to-kidney CNR on 120-kVp-MBIR images was higher than that on the VMS-ASIR images; however, future studies comparing 120-kVp-MBIR images with VMS images with MBIR would be desirable.

In conclusion, regardless of the reconstruction algorithm used, VMS images at 70 keV showed a lower degree of pseudoenhancement of renal cysts than 120-kVp images, while maintaining kidney contrast enhancement comparable to that on 120-kVp images; these findings could allow more accurate differentiation between renal cysts and solid masses.

ACKNOWLEDGMENTS

The authors thank Mayu Hiraiwa, Akihisa Yamazaki, Kazuya Minamishima, Mariko Shimizu, Yuki Niijima, and

Masakazu Hasegawa for their valuable assistance in the image collection, and Yasuhiro Imai and Kosuke Sasaki for their important suggestions.

REFERENCES

1. Bosniak MA. The current radiological approach to renal cysts. *Radiology.* 1986;158:1–10.
2. Chung EP, Herts BR, Linnell G, et al. Analysis of changes in attenuation of proven renal cysts on different scanning phases of triphasic MDCT. *AJR Am J Roentgenol.* 2004;182:405–410.
3. Sai V, Rakow-Penner R, Yeh BM, et al. Renal cyst pseudoenhancement at 16- and 64-dector row MDCT. *Clin imaging.* 2013;37:520–525.
4. Tappouni R, Kissane J, Sarwani N, et al. Pseudoenhancement of renal cysts: influence of lesion size, lesion location, slice thickness, and number of MDCT detectors. *AJR Am J Roentgenol.* 2012;198:133–137.
5. Bae KT, Heiken JP, Siegel CL, et al. Renal cysts: is attenuation artifactually increased on contrast-enhanced CT images? *Radiology.* 2000;216:792–796.
6. Maki DD, Birnbaum BA, Chakraborty DP, et al. Renal cyst pseudoenhancement: beam-hardening effects on CT numbers. *Radiology.* 1999;213:468–472.
7. Wang ZJ, Coakley FV, Fu Y, et al. Renal cyst pseudoenhancement at multidetector CT: what are the effects of number of detectors and peak tube voltage? *Radiology.* 2008;248:910–916.
8. Coulam CH, Sheafor DH, Leder RA, et al. Evaluation of pseudoenhancement of renal cysts during contrast-enhanced CT. *AJR Am J Roentgenol.* 2000;174:493–498.
9. Jinzaki M, McTavish JD, Zou KH, et al. Evaluation of small (</ = 3 cm) renal masses with MDCT: benefits of thin overlapping reconstructions. *AJR Am J Roentgenol.* 2004;183:223–228.
10. Birnbaum BA, Hindman N, Lee J, et al. Renal cyst pseudoenhancement: influence of multidetector CT reconstruction algorithm and scanner type in phantom model. *Radiology.* 2007;244:767–775.
11. Wu X, Langan DA, Xu D, et al. Monochromatic CT image representation via fast switching dual kVp. *Proc SPIE.* 2009;7258:725845.
12. Alvarez RE, Macovski A. Energy-selective reconstructions in X-ray computerized tomography. *Phys Med Biol.* 1976;21:733–744.
13. Lin XZ, Miao F, Li JY, et al. High-definition CT Gemstone spectral imaging of the brain: initial results of selecting optimal monochromatic image for beam-hardening artifacts and image noise reduction. *J Comput Assist Tomogr.* 2011;35:294–297.
14. Matsumoto K, Jinzaki M, Tanami Y, et al. Virtual monochromatic spectral imaging with fast kilovoltage switching: improved image quality as compared with that obtained with conventional 120-kVp CT. *Radiology.* 2011;259:257–262.
15. Dilmanian FA. Computed tomography with monochromatic x rays. *Am J Physiol Imaging.* 1992;7:175–193.
16. Silva AC, Morse BG, Hara AK, et al. Dual-energy (spectral) CT: applications in abdominal imaging. *Radiographics.* 2011;31:1031–1046.
17. Yamada Y, Jinzaki M, Tanami Y, et al. Virtual monochromatic spectral imaging for the evaluation of hypovascular hepatic metastases: the optimal monochromatic level with fast kilovoltage switching dual-energy computed tomography. *Invest Radiol.* 2012;47:292–298.
18. Yamada Y, Jinzaki M, Hosokawa T, et al. Abdominal CT: an intraindividual comparison between virtual monochromatic spectral and polychromatic 120-kVp images obtained during the same examination. *Eur J Radiol.* 2014;83:1715–1722.
19. Jung DC, Oh YT, Kim MD, et al. Usefulness of the virtual monochromatic image in dual-energy spectral CT for decreasing renal cyst pseudoenhancement: a phantom study. *AJR Am J Roentgenol.* 2012;199:1316–1319.
20. American Association of Physicists in Medicine. The measurement, reporting, and management of radiation dose in CT. January 2008. http://www.aapm.org/pubs/reports/rpt_96.pdf. Accessed February 15, 2014.
21. Yamada Y, Jinzaki M, Okamura T, et al. Feasibility of coronary artery calcium scoring on virtual unenhanced images derived from single-source fast kVp-switching dual-energy coronary CT angiography. *J Cardiovasc Comput Tomogr.* 2014;8:391–400.
22. Leipsic J, Labounty TM, Heilbron B, et al. Adaptive statistical iterative reconstruction: assessment of image noise and image quality in coronary CT angiography. *AJR Am J Roentgenol.* 2010;195:649–654.
23. Mitsumori LM, Shuman WP, Busey JM, et al. Adaptive statistical iterative reconstruction versus filtered back projection in the same patient: 64 channel liver CT image quality and patient radiation dose. *Eur Radiol.* 2012;22:138–143.
24. Sommer CM, Schwarzwaelder CB, Stiller W, et al. Dual-energy computed-tomography cholangiography in potential donors for living-related liver transplantation: initial experience. *Invest Radiol.* 2010;45:406–412.
25. Sommer CM, Schwarzwaelder CB, Stiller W, et al. Iodine removal in intravenous dual-energy CT-cholangiography: is virtual non-enhanced imaging effective to replace true non-enhanced imaging? *Eur J Radiol.* 2012;81:692–699.
26. Mileto A, Nelson RC, Samei E, et al. Impact of dual-energy multi-detector row CT with virtual monochromatic imaging on renal cyst pseudoenhancement: in vitro and in vivo study. *Radiology.* 2014:132856.
27. Birnbaum BA, Maki DD, Chakraborty DP, et al. Renal cyst pseudoenhancement: evaluation with an anthropomorphic body CT phantom. *Radiology.* 2002;225:83–90.
28. De Man B, Basu S. Distance-driven projection and backprojection in three dimensions. *Phys Med Biol.* 2004;49:2463–2475.
29. Whiting BR, Massoumzadeh P, Earl OA, et al. Properties of preprocessed sinogram data in x-ray computed tomography. *Med Phys.* 2006;33:3290–3303.
30. Bouman C, Sauer K. A generalized Gaussian image model for edge-preserving MAP estimation. *IEEE Trans Image Process.* 1993;2:296–310.
31. Yu Z, Thibault JB, Bouman CA, et al. Fast model-based X-ray CT reconstruction using spatially nonhomogeneous ICD optimization. *IEEE Trans Image Process.* 2011;20:161–175.
32. Yamada Y, Jinzaki M, Tanami Y, et al. Model-based iterative reconstruction technique for ultralow-dose computed tomography of the lung: a pilot study. *Invest Radiol.* 2012;47:482–489.
33. Singh S, Kalra MK, Do S, et al. Comparison of hybrid and pure iterative reconstruction techniques with conventional filtered back projection: dose reduction potential in the abdomen. *J Comput Assist Tomogr.* 2012;36:347–353.
34. Yamada Y, Jinzaki M, Hosokawa T, et al. Dose reduction in chest CT: comparison of the adaptive iterative dose reduction 3D, adaptive iterative dose reduction, and filtered back projection reconstruction techniques. *Eur J Radiol.* 2012;81:4185–4195.